

Better Together: Resnet-50 accuracy with 13x fewer parameters and at 3x speed

Utkarsh Nath

Tandon school of engineering
New York University
un270@nyu.edu

Shrinu Kushagra

David R. Cheriton School of Computer Science
University of Waterloo
skushagr@uwaterloo.ca

Abstract

Recent research on compressing deep neural networks has focused on reducing the number of parameters. Smaller networks are easier to export and deploy on edge-devices. We introduce *Adjoined networks* as a training approach that can compress and regularize any CNN-based neural architecture. Our one-shot learning paradigm trains both the original and the smaller networks together. The parameters of the smaller network are shared across both the architectures. For resnet-50 trained on Imagenet, we are able to achieve a $13.7x$ reduction in the number of parameters¹ and a $3x$ improvement in inference time without any significant drop in accuracy. For the same architecture on CIFAR-100, we are able to achieve a $99.7x$ reduction in the number of parameters and a $5x$ improvement in inference time. On both these datasets, the original network trained in the adjoint fashion gains about 3% in top-1 accuracy as compared to the same network trained in the standard fashion.

1 Introduction

Neural networks have achieved state-of-the art performance on computer vision such as classification, object detection [23], image segmentation [1] and many more. Since the introduction of Alexnet [17], neural architectures have progressively gone deeper with an increase in the number of parameters. This includes architectures like Resnet [9] and its many variants (xresnet [10], resnext [32, 13] etc.), Densenet [14], Inception networks [5] and many others.

While these networks achieve human-level performance on many tasks, their large size makes it difficult to deploy on many edge devices (like mobile phones, iot and embedded devices). Unlike cloud servers, these edge devices are constrained in terms of memory, compute and energy resources. A large network performs a lot of computations, consumes more energy and is difficult to transport and to update. A large network also has a high prediction time per image. This is constraint when real-time inference is needed. Thus, compressing neural networks while maintaining accuracy has received significant attention in the last few years.

Pruning - These techniques involve removing parameters (or weights) which satisfy some criteria. For example, in weight pruning, all the parameters whose values are below some pre-determined threshold are removed [8]. A natural extension of this is channel pruning [20] and filter pruning [19] where entire convolution channel or filter is removed according to some criteria. However, all of these methods involve multiple passes of pruning followed by fine-tuning and require a very long time to compress. Moreover, weight pruning doesn't give the benefit of faster inference times unless there is hardware support for fast sparse matrix multiplications.

¹For size comparison, we ignore the parameters in the last linear layer as it varies by dataset and are typically dropped during fine-tuning. Else, the reductions are $11.5x$ and $95x$ for imagenet and cifar-100 respectively.

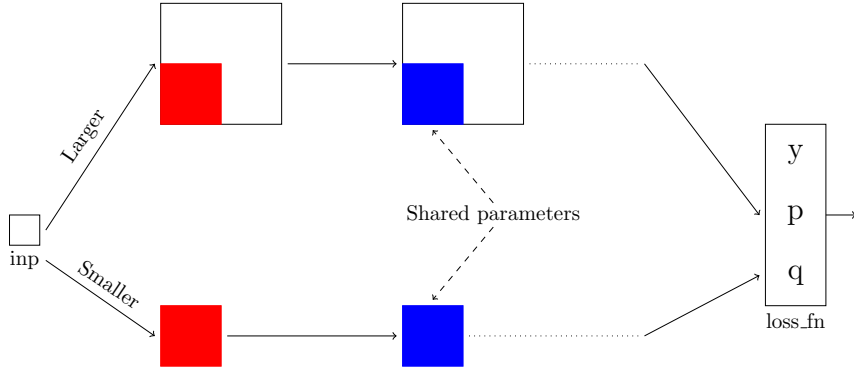


Figure 1: Training paradigm based on adjointed networks. The original and the compressed version of the network are trained together with the parameters of the smaller network shared across both. The network outputs two probability vectors p (original network) and q (corresponding to the smaller network).

Quantization and low-precision training - In quantization-based techniques, multiple parameters share the same value. Hence, only the effective values and their indices need to be stored [8]. This method of scalar quantization can be extended to vector quantization where a group of parameters share values [4]. In a recent work, [29] used a clustering based approach for vector quantization of resnet architectures. A similar approach is low-precision training where the goal is to train networks with integer or ternary or binary weights instead of floating point numbers [26, 21, 6]. As before, these techniques assume the availability of special hardware which supports fast inference.

Small architectures - Another approach is to design smaller architectures which can run efficiently on edge devices. SqueezeNet [15], MobileNet [25] and EfficientNet [31] to name a few. In this paper, our goal is to design a paradigm which can compress any architecture. Hence, the direction of architecture search is orthogonal to our approach.

To summarize, most of the current approaches suffer from one of the two problems. (1) Require the availability of special hardware to support fast inference. (2) Require huge training time as they alternate between pruning and fine-tuning. In this work, we propose a novel training paradigm based on *adjointed networks* which can compress any neural architecture, provides inference-time speedups and works at the application layer (does not require any specialized hardware).

As shown in Fig. 1, in the adjoint training paradigm, both the original and the compressed network are trained together at the same time. The parameters of the larger network are a super-set of the parameters of the smaller network. Details of our design, how it supports fast inference and relationship with other architectures (teacher-student [11], siamese networks [2], lottery ticket hypothesis [7]) are discussed in Section 2. In our training paradigm, we get two outputs p and q corresponding to the original and smaller networks respectively. We train the two networks using a novel time-dependent loss function, *adjoint loss* described in Section 3. The adjoint loss not only trains the smaller network but also acts as a regularizer for the bigger (original) network. We also show that training and regularizing in the adjoint fashion is better than other regularization techniques like dropouts [28].

In Section 4, we describe our results. We run several experiments on various datasets like ImageNet [24] and CIFAR-10 and CIFAR-100 [16]. For each of these datasets, we consider different architectures like resnet-50 and resnet-18. On CIFAR-100, the adjoint training paradigm allows to compress resnet-50 architecture by $99.7x$ without losing any accuracy. The compressed architecture has an inference speed of $5x$ when compared against the original, bigger architecture. Moreover, the original network gains 3.58% in accuracy when compared against the same network trained in the standard (non-adjoint) fashion. On the same dataset, for resnet-18, we achieve a compression factor of $49x$ at an inference speed of $3x$ with the bigger network gaining 5.55% accuracy (over the non-adjoint counterpart). On Imagenet, for resnet-50, we are able to compress it by $13.7x$ at an inference speed of $3x$. In this case, the bigger network gains 2.43% over its non-adjoint cousin clearly showing that it is **better** to train the networks **together**.

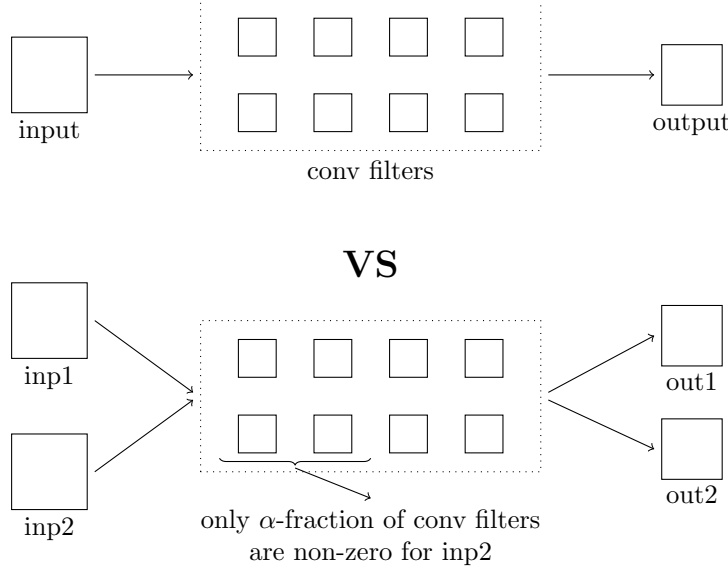


Figure 2: (Top) Standard 2d-convolution operation. The inputs, outputs and convolution filters are all 3d volumes. (Bottom) Adjoint convolution operation. The convolution layer receives two inputs inp1 and inp2. Standard convolution operation is applied on inp1 to get out1. For the second input, only a fraction of the conv filters are used (rest can be treated as zero or omitted) to get out2.

2 Adjoined networks

In our training paradigm the original (bigger) and the smaller network are trained together. The motivation for this kind of training comes from the principle that *good teachers are lifelong learners*. Hence, the bigger network which serves as a teacher for the smaller network should not be frozen (as in standard teacher-student architecture designs [11]). But rather both should learn together in a ‘combined learning environment’, that is, adjoined networks.² By learning together both the networks can be better together.

We are now ready to describe our approach and discuss the design of adjoined networks. But before that, let take a re-look at the standard convolution operator. Let $\mathbf{x} \in \mathbf{R}^{h \times w \times c_{in}}$ be the input to a convolution layer with weights $\mathbf{W} \in \mathbf{R}^{c_{out} \times h \times w \times c_{in}}$ where c_{in}, c_{out} denotes the number of input and output channels and h, w the height and width of the image. Then, we have that

$$\mathbf{y} = \text{conv}(\mathbf{W}, \mathbf{x})$$

In the adjoint paradigm, the weight matrix \mathbf{W} is the same as before but we now have two inputs \mathbf{x}_1 and \mathbf{x}_2 of size $h \times w \times c_{in}$. We get two outputs, as defined below.

$$\mathbf{y}_1 = \text{conv}(\mathbf{x}_1, \mathbf{W}) \quad \mathbf{y}_2 = \text{conv}(\mathbf{x}_2, \mathbf{W} * M) \quad (1)$$

Here $M \in \{0, 1\}^{c_{out} \times h \times w \times c_{in}}$ is binary mask of the same shape as \mathbf{W} and $*$ represents a point-wise multiplication. The framework of adjoined network places no restriction on the distribution of non-zero entries within the matrix M . For example, M could be a matrix *Rand* such that only $r\%$ of weights (chosen uniformly at randomly) are non-zero. In this paper, our intended application is to compress the smaller network to enable fast real-time inference. Hence, we use

$$M := \text{Adj-}\alpha = \underset{1}{\text{matrix such that only the first } \frac{c_{out}}{\alpha} \text{ filters are non-zero}} \quad (2)$$

In Section 4, we run experiments with *Adj- α* for $\alpha = \{4, 8, 16\}$. Also, note that the parameters of the matrix M are fixed before training and not learnt. From the purposes of compression, the only design choice is the parameter α (the fraction of filters to keep at each layer). Putting this all together, we see that any CNN-based architecture can be converted and trained in an adjoint fashion by replacing the standard convolution operation by the adjoint convolution operation (Eqn. 1). Since the first layer receives a single input (Fig. 1), two copies are created which are passed to the adjoined network. The network finally gives two outputs \mathbf{p} corresponding to the original (bigger or unmasked)

²Throughout the paper, we use the term adjoined networks and adjoint training paradigm interchangeably.

network and \mathbf{q} corresponding to the smaller (compressed) network where each convolution operation is done using a subset of the parameters described by the mask matrix M (or M_α). We train the network using a novel time-dependent loss function which forces \mathbf{p} and \mathbf{q} to be close to one another (Defn. 1). Before we describe our loss function in detail, we first compare our approach to other similar approaches and ideas in the literature.

Siamese networks is a neural network design that is used to compare two input vectors. Also called twin networks, they consist of two networks with identical parameters. Given two input vectors, the network returns two output vectors which are then used to compute the similarity between the input vectors [3]. More recently, siamese networks have been used in face verification [30]. The design of adjoined network also uses two architectures. However, both the architectures are not identical. Rather one is a super-set of the other. Also, rather than working on two different input vectors, adjoined networks work on a single input.

Lottery ticket hypothesis [7] says the following. A neural network contains within it a subset of parameters which are ‘special’. These 10 – 20% special parameters won the lottery during the network initialization process and it is possible to prune and train the original network to using only these special parameters. Thus, some weights in the network are just ‘lucky’ that they happened to be initialized in the ‘right’ way which made training possible with only these subsets of parameters. In our design, rather than relying on random initialization, we “force” some parameters to be special through the use of the mask matrix M and then training the two networks together through the adjoint-loss (Defn. 1).

3 One-shot regularization and compression

In the previous section, we looked at the design on adjoined networks. For one input $(\mathbf{X}, \mathbf{y}) \in \mathbf{R}^{h \times w \times c_{in}} \times [0, 1]^{n_c}$, the network outputs two vectors \mathbf{p} and $\mathbf{q} \in [0, 1]^{n_c}$ where n_c denotes the number of classes and c_{in} denotes the number of input channels (equals 3 for RGB images).

Definition 1 (Adjoint loss). *Let y be the ground-truth one-hot encoded vector and p and q be output probabilities by the adjoined network. Then*

$$\mathcal{L}(y, p, q) = -y \log p + \lambda(t) KL(p, q) \quad (3)$$

where $KL(p, q) = \sum_i p_i \log \frac{p_i}{q_i}$ is the measure of difference between two probability measures [18]. The regularization term $\lambda : [0, 1] \rightarrow \mathbf{R}$ is a function which changes with the number of epochs during training. Here $t = \frac{\text{current epoch}}{\text{Total number of epochs}}$ equals zero at the start of training and equals one at the end.

In our definition of loss function, the first term is the standard cross-entropy loss function which trains the bigger network. To train the smaller network, we use the predictions from the bigger network as a soft ground-truth signal. We use kl-divergence to measure how far the output of the smaller network is from the bigger network. This also has a regularizing effect as it forces the network to learn from a smaller set of parameters. Note that, in our implementations, we use $KL(p, q) = \sum p_i \log \frac{p_i + \epsilon}{q_i + \epsilon}$ to avoid rounding and division by zero errors where $\epsilon = 10^{-6}$.

At the start of training, p is not a reliable indicator of the ground-truth labels. To compensate for this, the regularization term λ changes with time. In our experiments, we used $\lambda(t) = \min\{4t^2, 1\}$. Thus, the contribution of the second term in the loss is zero at the beginning and steadily grows to one at 50% training. We experiment with different choices of the regularization function λ the results of which are in the appendix .

Comparison with dropout - Our idea of using only a subset of the parameters has some similarity to using dropouts where a fraction of the parameters are initialized to zero at training time. In this case, only the output of the smaller network is used to train the parameters. In our case, we use both the outputs. Our experiments show that training the networks together is a much more effective regularization strategy as compared to dropouts.

4 Experiments

We are now ready to describe our experiments in detail. We run experiments on five different datasets. (1) *Imagenet* - an image classification dataset [24] with 1000 classes and about 1.2M images . (2)

Adjoint-small vs standard						
Network	Dataset	Masking matrix (M)	Compression factor	Speed gain	top-1	top-5
Resnet-50	Cifar-10	Adj-8 * Rand(0.9)	88.9 x	4 x	-0.2	-0.06
	Cifar-100	Adj-16 * Rand(0.9)	99.6 x	4.7 x	-0.77	+2.13
	Imagenet	Adj-4	13.7 x	3.1 x	-1.37	-0.65
	Imagewoof	Adj-4 * Rand(0.8)	44.8 x	3.1 x	-0.44	+0.03
	Pets	Adj-4 * Rand(0.5)	24.15 x	3.1 x	+0.07	-0.07
Resnet-18	Cifar-10	Adj-16 * Rand(0.9)	68.7 x	2.6 x	-0.5	-0.06
	Cifar-100	Adj-4 * Rand(0.9)	48.9 x	2.1 x	+0.03	+1.51
	Imagewoof	Adj-4 * Rand(0.5)	21.8 x	2.1 x	-0.54	-0.31
	Pets	Adj-2 * Rand(0.5)	7.2 x	1.7 x	-1.22	-0.13

Table 1: The compression factor column is the ratio of number of parameters of the smaller network compared against the standard full network. The speed gain column denotes the ratio of inference time. The top-1 and top-5 columns show the difference of accuracies (in %). + denotes that the smaller adjoint network exceeds the accuracy of the standard full network and - denotes the opposite. Adj- α is as defined in Eqn. 2 and Rand(β) denotes a random matrix with β fraction of its entries are zero. * denotes dot-product. The absolute values can be found in the appendix .

CIFAR-10 - a collection of 60k images in 10 classes. (3) *CIFAR-100* - same as cifar-10 [16] but with 100 classes. (4) *Imagewoof* - A proxy dataset [12, 27] containing 10 different dog breeds from imagenet. (5) *Oxford-IIIT Pets* - a dataset [22] of pets containing 37 classes with approximately 200 images per class. For each of these datasets, we use standard data augmentation techniques like random-resize cropping, random flipping etc. The details are provided in the appendix .

We train two different architectures on all of the above datasets. Namely, resnet50 and resnet18. The detailed architecture diagram can be found in appendix material. On each dataset, we first train these architectures in the standard non-adjoint fashion using the cross-entropy loss function. We will refer to it by the name *standard* or *standard-full*. Next, we train the adjoint network, obtained by replacing the standard convolution operation by the adjoint convolution operation, using the adjoint loss function. In the second step, we obtain two different networks. In this section, we refer to them by *ajoint-full* and the *adjoint-small* networks. We compare the performance of the adjoint-full and adjoint-small networks against the standard network. One point to note is that we do not replace the convolutions in the stem layers but only those in the res-blocks. Since most of the weights are in the later layers, this leads to significant space and time savings while retaining competitive accuracy.

We ran our experiments on gpu enabled machine using pytorch. We trained all our networks using the adam optimizer with a cosine learning rate schedule with gradual warm-up. The parameters of the network were randomly initialized. Unless otherwise specified, we train both the standard and adjoint networks for the same number of epochs. We have also open-sourced our implementation ³.

In Section 4.1, we describe our results for compression. In Section 4.2, we show the strong regularizing effect of adjoint training. In Section 4.3, we compare our approach to dropouts, a popular approach to regularizing deep neural networks. Finally, in Section 4.4, we discuss various other choices for the regularization function in adjoint loss (Eqn. 3). In total, we ran close to 150 different experiments covering different datasets, different masking matrices etc. The detailed results are included in the appendix .

4.1 Compression

Table 1 compares the performance of the adjoint-small network against the performance of standard-full network. We use the Adj- α as the masking matrix (defined in Eqn. 2). The mask is such that the last $(1 - \frac{1}{\alpha})$ filters are zero. Hence, these can be pruned away to support fast inference. Using Adj- α

³The code can be found at <https://github.com/utkarshnath/Adjoint-Network.git>

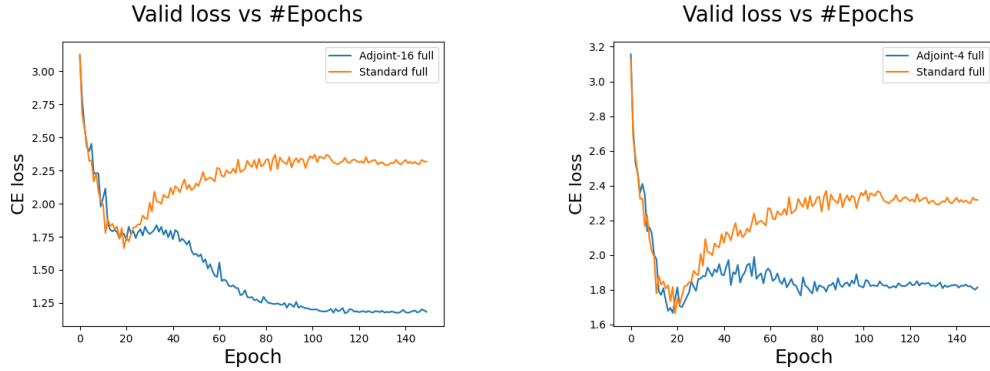


Figure 3: (Left) Plot of validation cross-entropy loss of the adjoint-16 full and standard resnet50 network on CIFAR-100. (Right) Plot of validation cross-entropy loss of the adjoint-4 full and standard resnet50 network on Imagenet

Adjoint-full vs standard				
Network	Dataset	Masking matrix (M)	top-1	top-5
Resnet-50	Cifar-10	Adj-16	1.09	0.04
	Cifar-100	Adj-16	3.76	3.76
	Imagenet	Adj-4	2.43	1.7
	Imagewoof	Adj-4 * Rand(0.9)	1.1	0.19
	Pets	Adj-2	1.7	0.4
Resnet-18	Cifar-10	Adj-8	2.1	0.31
	Cifar-100	Adj-4	5.45	3.82
	Imagewoof	Adj-4	0.81	0.08
	Pets	Adj-8	0.68	0.95

Table 2: The top-1 and top-5 columns show the difference of accuracies (in %) of the network trained in the adjoint fashion vs the same network trained in the standard way. In all cases the adjoint network exceeds the accuracy of the standard full network. Adj- α , Rand(β) are as in Table 1. The absolute values can be found in the appendix .

suffices for speed optimization. But, we can get a further reduction in the number of parameters, by multiplying the adjoint matrix by another random matrix Rand. This matrix is such that only a fraction of its entries are non-zero. Hence, using such a mask matrix further reduces the model size.

We also observe that resnet-50 is a bigger network and can be compressed more. Also, different datasets can be compressed by different amounts. For example, on cifar-10 and 100 datasets, the network can be compressed by factors $\sim 90x$ while for other datasets it ranges from $7x$ to $44x$. Our goal is to compare the adjoint models against the standard models. Hence, we only report the difference in accuracies. The absolute numbers can be found in the appendix . Note that in all the cases, the drop in accuracy is small, a maximum of -1.4% over all the datasets. In some cases, the smaller network even outperforms (ever so slightly) the bigger network.

4.2 Regularization

Table 2 compares the performance of the adjoint-full network against the performance of the corresponding standard-full network. We see a consistent trend that the network trained adjointly outperforms the same network trained in the standard way. We see maximum gains on cifar-100, exceeding accuracies by as much as 5.5%. Even on imagenet, we see a gain of about 2.5%. Fig. 3 shows the plot of validation cross-entropy loss as a function of the number of epochs. For a fair comparison, we look at the $-y \log p$ (Eqn. 3) term of the adjoint loss function. By regularizing the

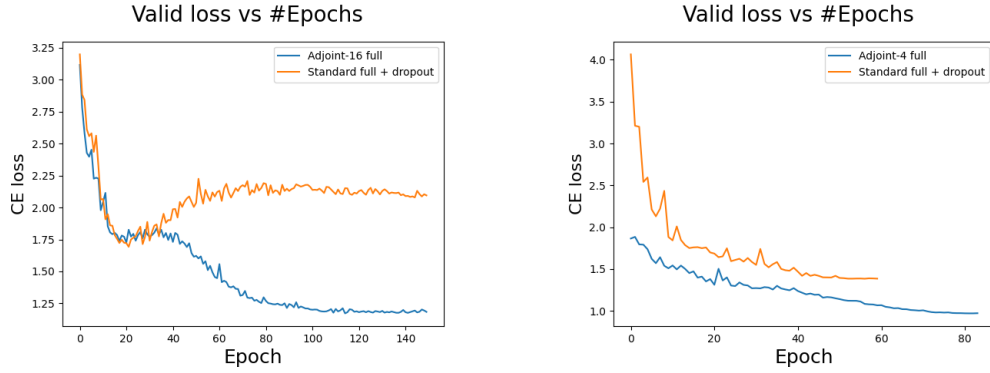


Figure 4: (Left) Plot of validation cross-entropy loss of the adjoint-16 full and standard + dropout resnet50 network on CIFAR-100. (Right) Plot of validation cross-entropy loss of the adjoint-4 full and standard + dropout resnet50 network on Imagenet

Adjoint-full vs standard-full + dropouts				
Network	Dataset	Masking matrix (M)	top-1	top-5
Resnet-50	Cifar-10	Adj-16	1.23	0.03
	Cifar-100	Adj-16	2.41	2.87
	Imagenet	Adj-4	6.3	3.4
	Imagewoof	Adj-4 * Rand(0.9)	3.54	0.21
	Pets	Adj-4	2.03	0.14
Resnet-18	Cifar-10	Adj-8	122	0.17
	Cifar-100	Adj-4	2.54	1.07
	Imagewoof	Adj-4	2.06	0.29
	Pets	Adj-8	2.91	1.62

Table 3: The top-1 and top-5 columns show the difference of accuracies (in %) of the network trained in the adjoint fashion vs the same network trained in the standard way using droupouts In all cases the adjoint network exceeds the accuracy of the standard one. Adj- α , Rand(β) are as in Table 1. The absolute values can be found in the appendix .

loss function, we are able to train longer while decreasing the loss function. On the other hand, the network trained in the standard fashion starts to over-fit after a while (as evident in the loss profile). Fig. 3 shows the loss plot on one architecture for two datasets. Similar plots on other datasets and for other architectures are available in the appendix .

4.3 Comparison against dropouts

Table 3 compares the performance of the adjoint-full network against the performance of the corresponding standard-full network where the standard network was trained using dropouts. We see a consistent trend that the network trained adjointly outperforms the same network trained with dropout regularization. We see maximum gains on imagenet, exceeding accuracies by as much as 6.3%. On cifar and imagewoof, we see gains of about 3%. As is evident from our experiments, dropouts are not very effective regularizers on the imagenet dataset. This is one of the reasons why they have been going out-of-fashion on vision tasks. Fig. 4 shows the plot of validation cross-entropy loss as a function of the number of epochs. As before, we only look at the $-y \log p$ (Eqn. 3) term. The above results show that adjoint training is much more effective regularization strategy as compared against dropouts. Similar plots on other datasets and for other architectures are available in the appendix .

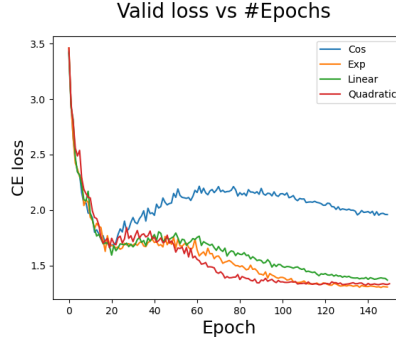


Figure 5: Validation cross entropy loss for various regularization functions. The networks were trained using Adj-4 mask matrix on cifar-100 using resnet-18.

Adjoint trained with different regularization functions		
Regularization function $\lambda(t)$	top-1 full	top-1 small
$1 - \cos(t)$	-2.86	-3.14
t	-0.1	-0.15
$\min\{4t^2, 1\}$	0.00	0.00
$\exp(t) - 1$	-0.37	+0.38

Table 4: The effect of training with different regularization functions on the top-1 accuracies of the bigger and the smaller networks. The quadratic function $\min\{4t^2, 1\}$ is used as the base for comparison.

4.4 Choosing the regularization function

Finally, we compare different choices of regularization function for the adjoint loss (Eqn. 3). For all the previous experiments, we use the ‘quadratic’ function $\lambda(t) = \min\{4t^2, 1\}$. In this section, we fix the architecture, dataset and mask matrix as resnet18, cifar100 and Adj-4 respectively and vary the regularization function. We look at different functions which includes exponential and trigonometric functions. Table 4 and Fig. 5 both show the same trend. The cos function performs the worst while the rest have similar performance. We conjecture that any function that is close to zero for $t \leftarrow 0$ and grows to one eventually should be a reasonable choice for the regularization function. Note that throughout our discussion, we have used $\lambda(t) = c \min\{4t^2, 1\}$ with $c = 1$. Depending on the dataset, other values of c maybe more appropriate.

5 Conclusion and future work

In this work, we introduced the paradigm of Adjoined network training. We showed how this approach to training neural networks can allow us to compress large networks like Resnet-50 by $13x$, (even going up to $99.7x$ on some datasets) while retaining the accuracy. We showed that the idea of adjoining two networks together can be used to regularize any architecture. We showed that adjoining a large and a small network together enables the large network to significantly exceed its own accuracy (when trained in the standard way) and is a much more effective regularization strategy than dropouts. Based on our experiments, we propose that adjoint networks be used as a regularization tool for all deep architectures.

In this work, our focus was on image classification tasks. As an immediate next step, we are applying the paradigm of adjoined networks to other problems like object detection and segmentation. Architectures for these tasks often use an ‘upsampling’ layer (ex. deconvolution). It will be interesting to see how adjoining effects model accuracy for such architectures. Another very interesting direction of research is to apply adjoint training for RNN-based architectures in nlp. Is it possible to replace dropouts in rnn architectures with adjoint networks?

6 Broader impact of this work

Deep learning models are getting bigger and bigger. Popular architectures like resnet50 have 20 million parameters; bert, a popular language model has 340 million parameters. There are countless examples of huge models being trained to move the state-of-the-art by a fractional percentage points on many datasets. If we envision a world where deep learning is being used to solve the problems of human society, most of this intelligence will live on the edge on devices like mobile phones, iot devices, drones etc. Such devices are heavily compute and size constrained as compared against the server on which the models are usually trained on. For companies trying to democratize access to deep learning technologies, model compression is a very important problem.

However, there is no consensus on the right approach for compression. All the current techniques require a very long training time and require hardware based optimizations. The process is so cumbersome that companies have dedicated teams of multiple people (sometimes even tens of people) involved in model compression. In this work, we propose an end-to-end, one-shot and simple-to-implement compression approach. We believe that our approach will enable hundreds of deep learning engineers and developers easily compress and deploy their models.

While the motivation for our approach was compression, we found that it has great benefits for model regularization., significantly outperforming dropouts in all our experiments. We believe that *training by adjoining* will form part of the standard toolkit of regularization strategies for deep learning.

References

- [1] V. Badrinarayanan, A. Kendall, and R. Cipolla. Segnet: A deep convolutional encoder-decoder architecture for image segmentation. *IEEE transactions on pattern analysis and machine intelligence*, 39(12):2481–2495, 2017.
- [2] L. Bertinetto, J. Valmadre, J. F. Henriques, A. Vedaldi, and P. H. Torr. Fully-convolutional siamese networks for object tracking. In *European conference on computer vision*, pages 850–865. Springer, 2016.
- [3] J. Bromley, I. Guyon, Y. LeCun, E. Säckinger, and R. Shah. Signature verification using a "siamese" time delay neural network. In *Advances in neural information processing systems*, pages 737–744, 1994.
- [4] M. A. Carreira-Perpinán and Y. Idelbayev. Model compression as constrained optimization, with application to neural nets. part ii: Quantization. *arXiv preprint arXiv:1707.04319*, 2017.
- [5] L.-C. Chen, G. Papandreou, F. Schroff, and H. Adam. Rethinking atrous convolution for semantic image segmentation. *arXiv preprint arXiv:1706.05587*, 2017.
- [6] M. Courbariaux, Y. Bengio, and J.-P. David. Binaryconnect: Training deep neural networks with binary weights during propagations. In *Advances in neural information processing systems*, pages 3123–3131, 2015.
- [7] J. Frankle and M. Carbin. The lottery ticket hypothesis: Finding sparse, trainable neural networks. *arXiv preprint arXiv:1803.03635*, 2018.
- [8] S. Han, H. Mao, and W. J. Dally. Deep compression: Compressing deep neural networks with pruning, trained quantization and huffman coding. *arXiv preprint arXiv:1510.00149*, 2015.
- [9] K. He, X. Zhang, S. Ren, and J. Sun. Deep residual learning for image recognition. In *Proceedings of the IEEE conference on computer vision and pattern recognition*, pages 770–778, 2016.
- [10] T. He, Z. Zhang, H. Zhang, Z. Zhang, J. Xie, and M. Li. Bag of tricks for image classification with convolutional neural networks. In *Proceedings of the IEEE Conference on Computer Vision and Pattern Recognition*, pages 558–567, 2019.
- [11] G. Hinton, O. Vinyals, and J. Dean. Distilling the knowledge in a neural network. *arXiv preprint arXiv:1503.02531*, 2015.
- [12] J. Howard. Imagenette. URL: *Github repository with links to dataset.* <https://github.com/fastai/imagenette>, 2019.
- [13] J. Hu, L. Shen, and G. Sun. Squeeze-and-excitation networks. In *Proceedings of the IEEE conference on computer vision and pattern recognition*, pages 7132–7141, 2018.

- [14] G. Huang, Z. Liu, L. Van Der Maaten, and K. Q. Weinberger. Densely connected convolutional networks. In *Proceedings of the IEEE conference on computer vision and pattern recognition*, pages 4700–4708, 2017.
- [15] F. N. Iandola, S. Han, M. W. Moskewicz, K. Ashraf, W. J. Dally, and K. Keutzer. Squeezenet: Alexnet-level accuracy with 50x fewer parameters and < 0.5 mb model size. *arXiv preprint arXiv:1602.07360*, 2016.
- [16] A. Krizhevsky, V. Nair, and G. Hinton. Cifar-10 and cifar-100 datasets. *URL: <https://www.cs.toronto.edu/kriz/cifar.html>*, 6, 2009.
- [17] A. Krizhevsky, I. Sutskever, and G. E. Hinton. Imagenet classification with deep convolutional neural networks. In *Advances in neural information processing systems*, pages 1097–1105, 2012.
- [18] S. Kullback and R. A. Leibler. On information and sufficiency. *The annals of mathematical statistics*, 22(1):79–86, 1951.
- [19] H. Li, A. Kadav, I. Durdanovic, H. Samet, and H. P. Graf. Pruning filters for efficient convnets. *arXiv preprint arXiv:1608.08710*, 2016.
- [20] Z. Liu, J. Li, Z. Shen, G. Huang, S. Yan, and C. Zhang. Learning efficient convolutional networks through network slimming. In *Proceedings of the IEEE International Conference on Computer Vision*, pages 2736–2744, 2017.
- [21] M. D. McDonnell. Training wide residual networks for deployment using a single bit for each weight. *arXiv preprint arXiv:1802.08530*, 2018.
- [22] O. M. Parkhi, A. Vedaldi, A. Zisserman, and C. Jawahar. Cats and dogs. In *2012 IEEE conference on computer vision and pattern recognition*, pages 3498–3505. IEEE, 2012.
- [23] J. Redmon, S. Divvala, R. Girshick, and A. Farhadi. You only look once: Unified, real-time object detection. In *Proceedings of the IEEE conference on computer vision and pattern recognition*, pages 779–788, 2016.
- [24] O. Russakovsky, J. Deng, H. Su, J. Krause, S. Satheesh, S. Ma, Z. Huang, A. Karpathy, A. Khosla, M. Bernstein, A. C. Berg, and L. Fei-Fei. ImageNet Large Scale Visual Recognition Challenge. *International Journal of Computer Vision (IJCV)*, 115(3):211–252, 2015.
- [25] M. Sandler, A. Howard, M. Zhu, A. Zhmoginov, and L.-C. Chen. Mobilenetv2: Inverted residuals and linear bottlenecks. In *Proceedings of the IEEE conference on computer vision and pattern recognition*, pages 4510–4520, 2018.
- [26] O. Shayer, D. Levi, and E. Fetaya. Learning discrete weights using the local reparameterization trick. *arXiv preprint arXiv:1710.07739*, 2017.
- [27] S. Shleifer and E. Prokop. Using small proxy datasets to accelerate hyperparameter search. *arXiv preprint arXiv:1906.04887*, 2019.
- [28] N. Srivastava, G. Hinton, A. Krizhevsky, I. Sutskever, and R. Salakhutdinov. Dropout: a simple way to prevent neural networks from overfitting. *The journal of machine learning research*, 15(1):1929–1958, 2014.
- [29] P. Stock, A. Joulin, R. Gribonval, B. Graham, and H. Jégou. And the bit goes down: Revisiting the quantization of neural networks. *arXiv preprint arXiv:1907.05686*, 2019.
- [30] Y. Taigman, M. Yang, M. Ranzato, and L. Wolf. Deepface: Closing the gap to human-level performance in face verification. In *Proceedings of the IEEE conference on computer vision and pattern recognition*, pages 1701–1708, 2014.
- [31] M. Tan and Q. V. Le. Efficientnet: Rethinking model scaling for convolutional neural networks. *arXiv preprint arXiv:1905.11946*, 2019.
- [32] S. Xie, R. Girshick, P. Dollár, Z. Tu, and K. He. Aggregated residual transformations for deep neural networks. In *Proceedings of the IEEE conference on computer vision and pattern recognition*, pages 1492–1500, 2017.

A Data augmentation

We use different data-augmentation techniques for different datasets. Below are the details.

- *Cifar-10, Cifar-100 and Oxford pets*

We apply the following set of transforms for these datasets. (1) We flip the image with probability 0.5. (2) With probability 0.75, we rotate the image by degree d chosen uniformly at random from $(-max_d, max_d)$. $max_d = 25.0$ for the cifar datasets and $max_d = 10.0$ for the pets dataset. (3) With probability 0.75, we apply the contrast and brightness transforms. (4) With probability 0.75, we apply the warp and zoom transforms. (5) We normalize the image by first dividing all the pixel values by 255. and then subtracting the mean $[0.485, 0.456, 0.406]$ and dividing by the variance $[0.229, 0.224, 0.225]$.

- *Imagenet and Imagewoof*

On these two datasets, we apply the following set fo transforms. (1) Random resize cropping - Crop a rectangular region with aspect ratio in $[3/4, 4/3]$ (selected uniformly at random) with area in $[0.08, 1.0]$ of the original area. (2) Flip the image horizontally with probability 0.5. (3) Normalize the image by dividing all pixel values of 255.0.

For cifar-10 and cifar-100, input size is 32×32 for all the other datasets, the input size is 224×224 . The above transforms are applicable for the training dataset. For validation, we use center crop - select the center of the image with 85% area, followed by a normalization step. Note that our data augmentation are not heavily optimized for accuracy. Rather our goal is to compare adjoint training with standard training. Hence, we use the same data augmentation steps for both the trainings. For standard training, our accuracies are still comparable to the accuracies reported in the literature on these datasets using the resnet18 and resnet50 architectures. However, the adjoint training methodology proposed in this paper outperforms the network trained in the standard way.

More details of the data-augmentation can be found in the code in the github repository.

B Resnet architecture diagram

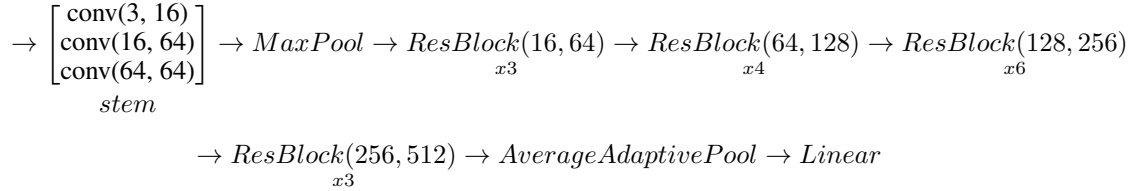


Figure 6: Architecture diagram for resnet50 network used in this paper. $\text{conv}(ni, no)$ is a combination of convolution layer with ni input and no output channels followed by a batch norm and relu layer. The ResBlocks are as defined in Fig. 7.

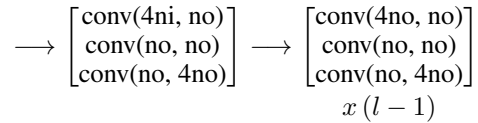


Figure 7: A ResBlock with l layers and input ni and output no .

The architecture for resnet50 is depicted in Figs. 6 and 7. Each conv layer is actually a combination of three layers. A standard convolution layer followed by a batch normalization layer followed by a relu activation. The *ResBlock* refers to the residual blocks in resnet architecture. Note that the skip connections are not shown in these diagrams. For a resnet18 architecture, each resblock is repeated twice instead of 3, 4, 6 and 3 times. Also, the resblock does not have a factor four in the convolution input and output.

For adjoint networks, the convolution parameters of all the last three resblocks are shared across both the original and the smaller architecture. Note that both the networks have different parameters for the batch-norm layers.

C Detailed experimental results

C.1 Experiments on cifar-10

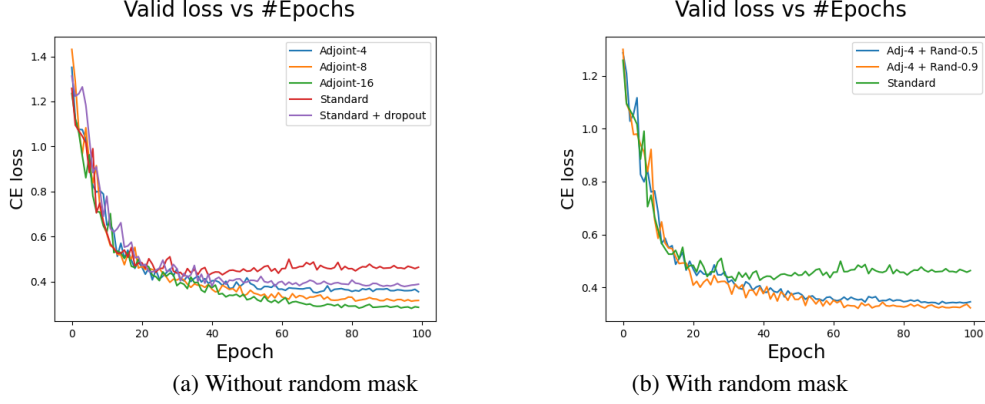


Figure 8: Validation loss for the various training paradigms for resnet50 trained on Cifar-10. All the adjoint plots correspond to the bigger network.

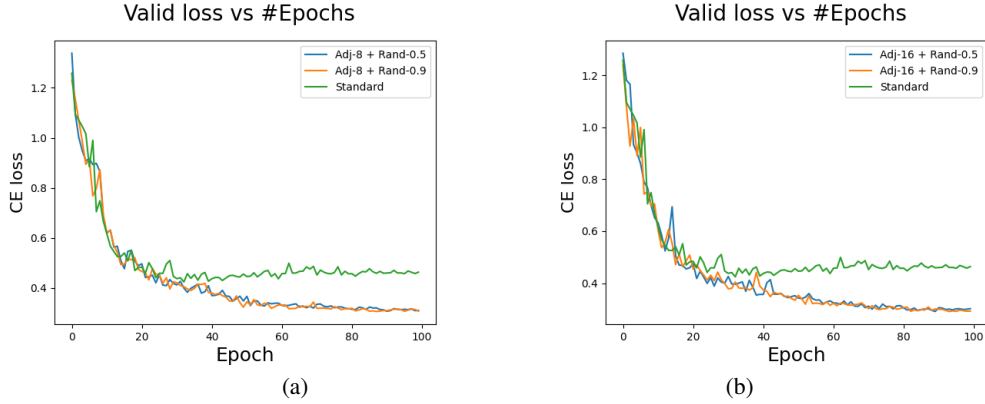


Figure 9: Validation loss for the various training paradigms for resnet50 trained on Cifar-10. Validation loss for the various training paradigms for resnet50 trained on Cifar-10. All the adjoint plots correspond to the bigger network.

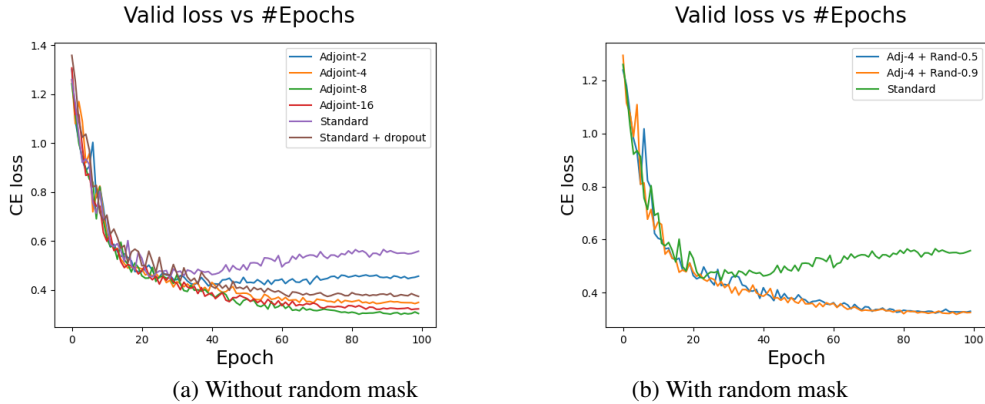


Figure 10: Validation loss for the various training paradigms for resnet18 trained on Cifar-10. All the adjoint plots correspond to the bigger network.

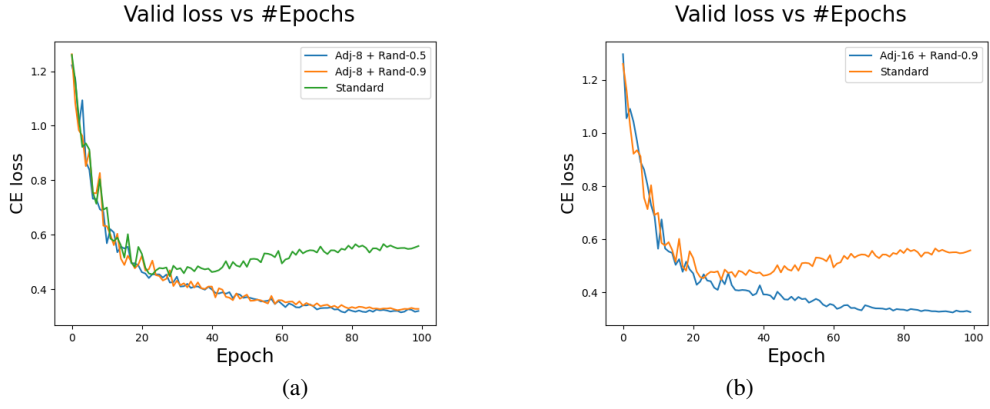


Figure 11: Validation loss for the various training paradigms for resnet18 trained on Cifar-10. All the adjoint plots correspond to the bigger network.

Training with resnet50 on cifar-10					
Training paradigm	Masking matrix (M)	top-1 full	top-5 full	top-1 small	top-5 small
Standard-full		90.25	99.67		
Standard-full + dropout (0.75)		90.11	99.68		
Adjoint-4	Adj-4	90.83	99.7	90.25	99.6
Adjoint-8	Adj-8	91.06	99.67	89.77	99.63
Adjoint-16	Adj-16	91.34	99.71	89.88	99.61
Adjoint-4	Adj-4 * Rand(0.5)	90.56	99.75	90.13	99.73
Adjoint-4	Adj-4 * Rand(0.9)	91.12	99.69	90.1	99.7
Adjoint-8	Adj-8 * Rand(0.5)	91.01	99.77	89.64	99.71
Adjoint-8	Adj-8 * Rand(0.9)	91.31	99.73	90.05	99.61
Adjoint-16	Adj-16 * Rand(0.5)	91.13	99.59	89.81	99.63
Adjoint-16	Adj-16 * Rand(0.9)	91.2	99.68	89.42	99.61

Table 5: Accuracy for the various training paradigms for resnet50 trained on Cifar-10

Training with resnet18 on cifar-10					
Training paradigm	Masking matrix (M)	top-1 full	top-5 full	top-1 small	top-5 small
Standard-full		88.17	99.41		
Standard-full + dropout (0.5)		89.04	99.55		
Adjoint-2	Adj-2	88.75	99.54	88.06	99.41
Adjoint-4	Adj-4	89.8	99.73	88.74	99.64
Adjoint-8	Adj-8	90.26	99.72	88.62	99.62
Adjoint-16	Adj-16	89.58	99.61	87.94	99.57
Adjoint-4	Adj-4 * Rand(0.5)	89.88	99.65	88.59	99.53
Adjoint-4	Adj-4 * Rand(0.9)	89.75	99.56	88.34	99.48
Adjoint-8	Adj-8 * Rand(0.5)	89.96	99.61	87.85	99.52
Adjoint-8	Adj-8 * Rand(0.9)	89.4	99.56	87.61	99.51
Adjoint-16	Adj-16 * Rand(0.9)	89.66	99.52	87.67	99.35

Table 6: Accuracy for the various training paradigms for resnet18 trained on Cifar-10

C.2 Experiments on cifar-100

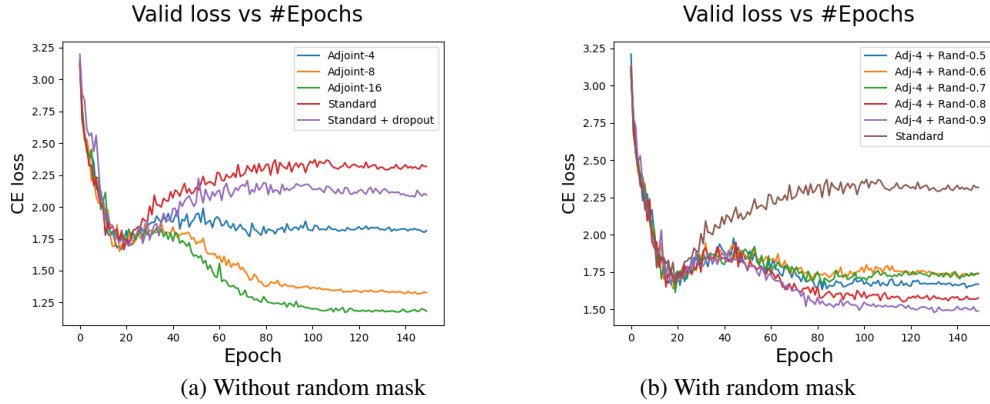


Figure 12: Validation loss for the various training paradigms for resnet50 trained on Cifar-100. All the adjoint plots correspond to the bigger network.

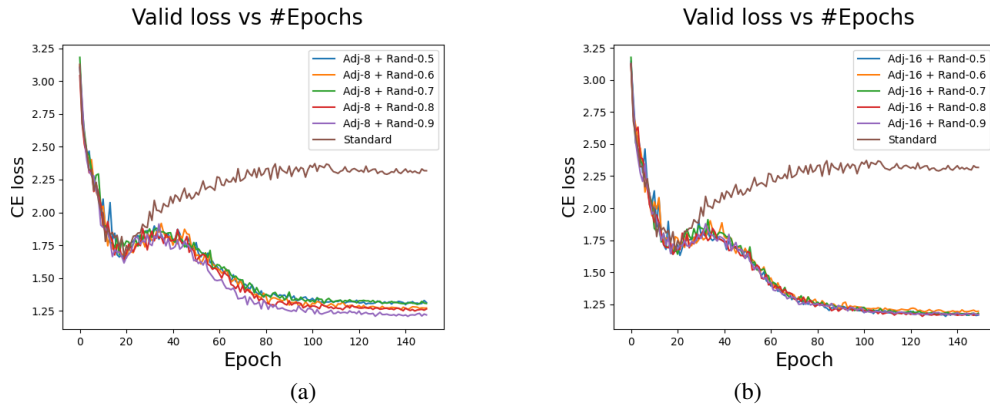


Figure 13: Validation loss for the various training paradigms for resnet50 trained on Cifar-100. All the adjoint plots correspond to the bigger network.

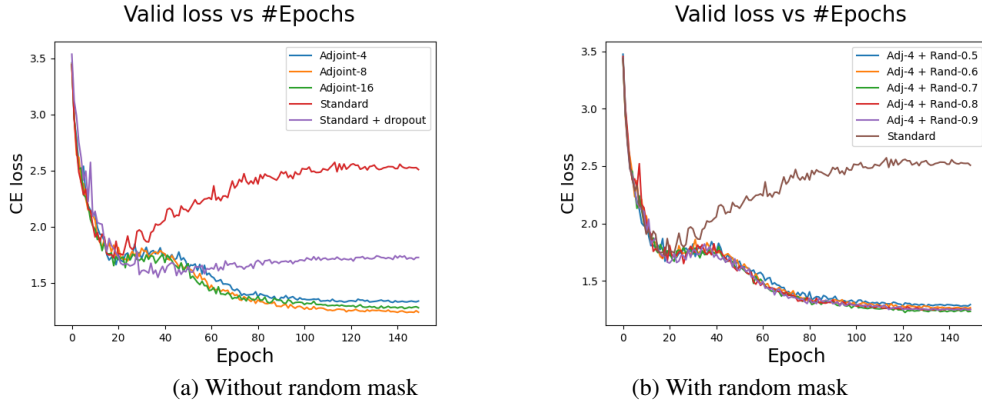


Figure 14: Validation loss for the various training paradigms for resnet18 trained on Cifar-100. All the adjoint plots correspond to the bigger network.

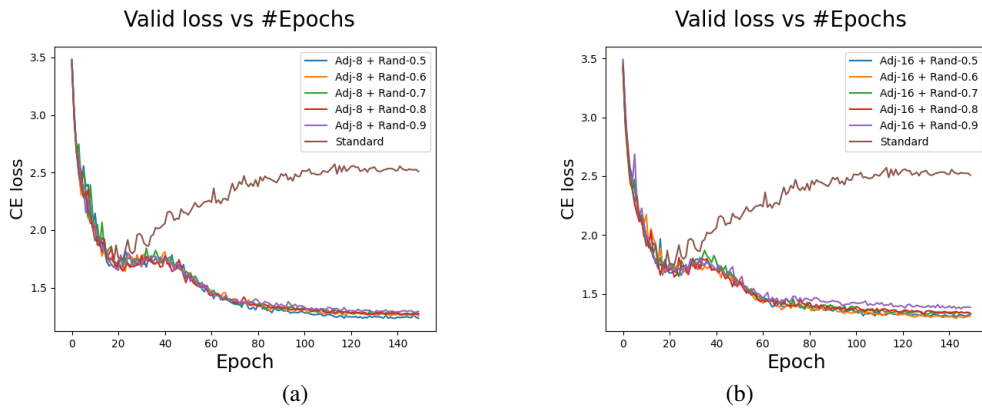


Figure 15: Validation loss for the various training paradigms for resnet18 trained on Cifar-100. All the adjoint plots correspond to the bigger network.

Training with resnet50 on cifar-100					
Training paradigm	Masking matrix (M)	top-1 full	top-5 full	top-1 small	top-5 small
Standard-full		65.31	87.35		
Standard-full + dropout (0.75)		66.66	88.24		
Adjoint-4	Adj-4	67.15	89.04	64.73	87.6
Adjoint-8	Adj-8	68.75	90.79	65.37	88.88
Adjoint-16	Adj-16	69.07	91.11	65.11	89.08
Adjoint-4	Adj-4 * Rand(0.5)	67.47	89.78	64.71	88.12
Adjoint-4	Adj-4 * Rand(0.6)	67.45	89.22	64.56	87.56
Adjoint-4	Adj-4 * Rand(0.7)	67.35	89.69	64.26	87.84
Adjoint-4	Adj-4 * Rand(0.8)	67.82	89.71	64.71	88.13
Adjoint-4	Adj-4 * Rand(0.9)	67.57	89.99	65.04	88.24
Adjoint-8	Adj-8 * Rand(0.5)	68.7	90.57	65.35	89.05
Adjoint-8	Adj-8 * Rand(0.6)	68.86	90.68	65.47	89.27
Adjoint-8	Adj-8 * Rand(0.7)	68.57	90.71	64.76	88.6
Adjoint-8	Adj-8 * Rand(0.8)	67.82	89.84	64.76	88.01
Adjoint-8	Adj-8 * Rand(0.9)	69.09	90.99	65.11	89.13
Adjoint-16	Adj-16 * Rand(0.5)	68.59	91.13	64.53	89.1
Adjoint-16	Adj-16 * Rand(0.6)	68.04	90.79	64.55	88.66
Adjoint-16	Adj-16 * Rand(0.7)	68.85	91.03	64.76	88.99
Adjoint-16	Adj-16 * Rand(0.8)	68.52	90.93	64.35	89.29
Adjoint-16	Adj-16 * Rand(0.9)	68.89	90.79	64.54	89.48

Table 7: Accuracy for the various training paradigms for resnet50 trained on Cifar-100

Training with resnet18 on cifar-100					
Training paradigm	Masking matrix (M)	top-1 full	top-5 full	top-1 small	top-5 small
Standard-full		61.39	85.38		
Standard-full + dropout (0.5)		64.3	88.13		
Adjoint-4	Adj-4	66.84	89.2	62.73	87.4
Adjoint-8	Adj-8	66.09	89.43	61.38	87.12
Adjoint-16	Adj-16	64.48	89.02	57.84	85.24
Adjoint-4	Adj-4 * Rand(0.5)	66.54	89.56	62.64	87.38
Adjoint-4	Adj-4 * Rand(0.6)	65.81	89.49	62.26	87.52
Adjoint-4	Adj-4 * Rand(0.7)	65.88	89.75	61.7	87.53
Adjoint-4	Adj-4 * Rand(0.8)	66.13	89.55	61.91	87.08
Adjoint-4	Adj-4 * Rand(0.9)	66.29	89.55	61.42	86.89
Adjoint-8	Adj-8 * Rand(0.5)	65.63	89.28	60.64	86.79
Adjoint-8	Adj-8 * Rand(0.6)	65.14	89.08	60.08	86.39
Adjoint-8	Adj-8 * Rand(0.7)	64.49	89.03	58.93	85.63
Adjoint-8	Adj-8 * Rand(0.8)	64.88	89.17	59.45	86.09
Adjoint-8	Adj-8 * Rand(0.9)	64.34	88.54	58.17	85.15
Adjoint-16	Adj-16 * Rand(0.5)	63.66	88.38	56.22	84.68
Adjoint-16	Adj-16 * Rand(0.6)	64.07	88.27	56.83	84.22
Adjoint-16	Adj-16 * Rand(0.7)	63.14	88.02	54.78	83.65
Adjoint-16	Adj-16 * Rand(0.8)	63.26	87.85	54.52	83.2
Adjoint-16	Adj-16 * Rand(0.9)	62.32	87.37	52.88	82.13

Table 8: Accuracy for the various training paradigms for resnet18 trained on Cifar-100

C.3 Experiments on imagenet

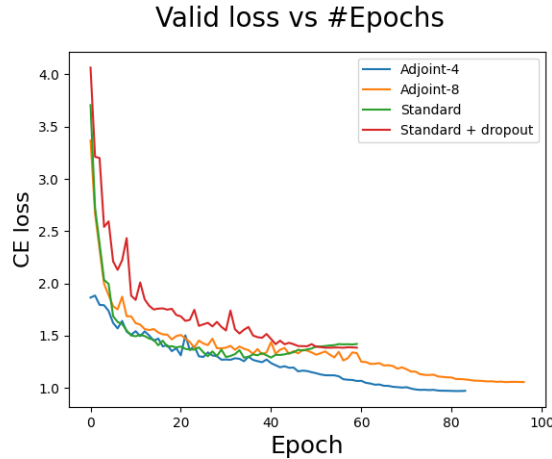


Figure 16: Validation loss for the various training paradigms for resnet50 trained on Imagenet. All the adjoint plots correspond to the bigger network.

Training with resnet50 on imagenet					
Training paradigm	Masking matrix (M)	top-1 full	top-5 full	top-1 small	top-5 small
Standard-full		73.41	91.07		
Standard-full + dropout (0.75)		69.54	88.88		
Adjoint-4	Adj-4	75.84	92.77	71.84	90.42
Adjoint-8	Adj-8	73.46	91.52	64.7	85.96

Table 9: Accuracy for the various training paradigms for resnet50 trained on imagenet

C.4 Experiments on imagewoof

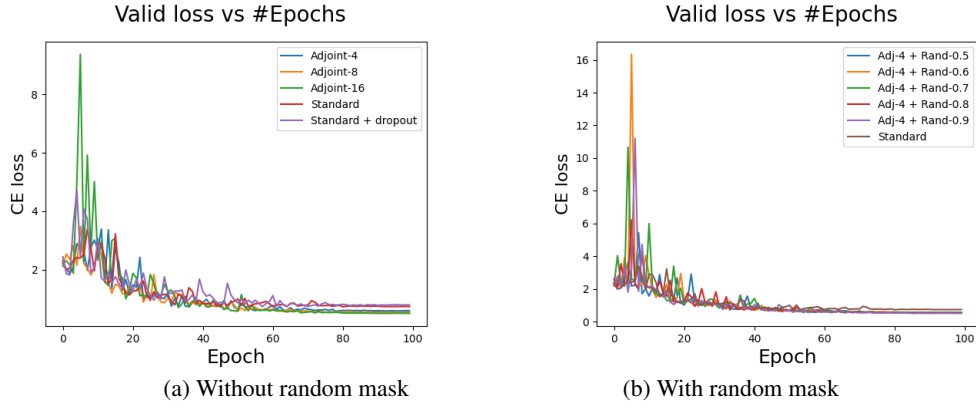


Figure 17: Validation loss for the various training paradigms for resnet50 trained on imagewoof. All the adjoint plots correspond to the bigger network.

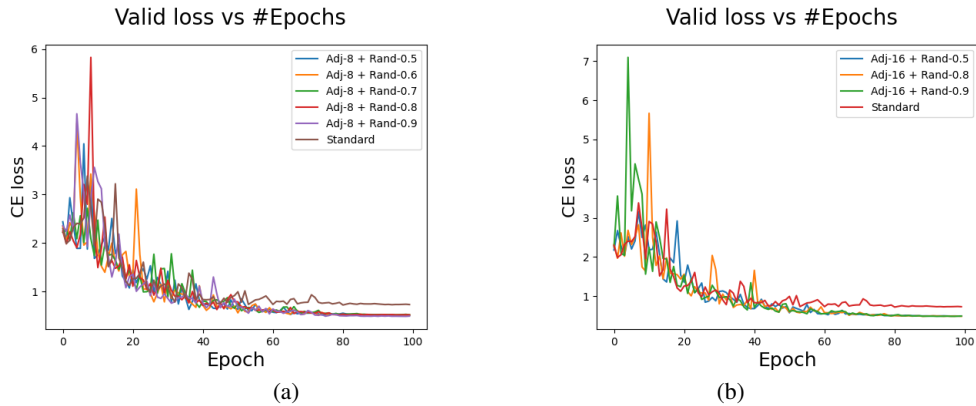


Figure 18: Validation loss for the various training paradigms for resnet50 trained on imagewoof. All the adjoint plots correspond to the bigger network.

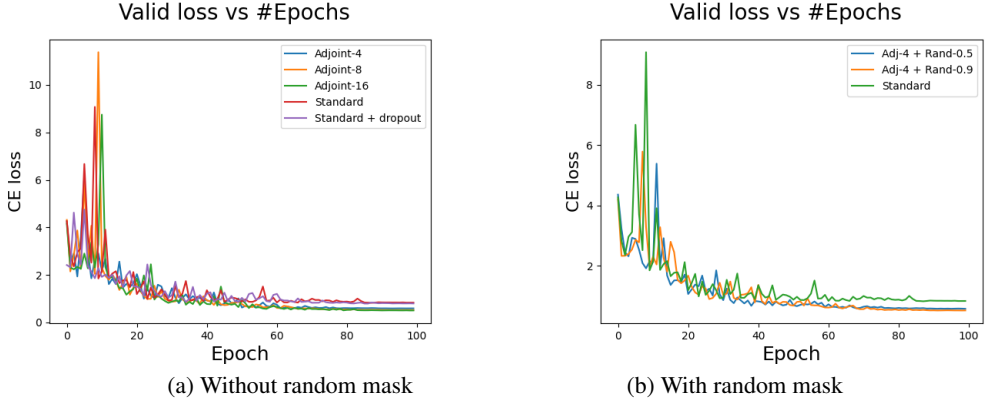


Figure 19: Validation loss for the various training paradigms for resnet18 trained on imagewoof. All the adjoint plots correspond to the bigger training network.

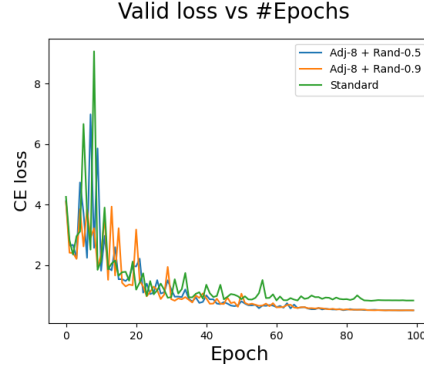


Figure 20: Validation loss for the various training paradigms for resnet18 trained on imagewoof. All the adjoint plots correspond to the bigger network.

Training with resnet18 on imagewoof					
Training paradigm	Masking matrix (M)	top-1 full	top-5 full	top-1 small	top-5 small
Standard-full		83.35	98.3		
Standard-full + dropout (0.5)		82.1	98.09		
Adjoint-4	Adj-4	84.16	98.38	82.96	98.3
Adjoint-8	Adj-8	84.11	98.54	81.25	98.02
Adjoint-16	Adj-16	83.59	98.43	79.37	97.78
Adjoint-4	Adj-4 * Rand(0.5)	84.14	98.48	82.81	97.99
Adjoint-4	Adj-4 * Rand(0.9)	83.82	98.17	80.54	98.02
Adjoint-8	Adj-8 * Rand(0.5)	84.27	98.69	81.69	98.28
Adjoint-8	Adj-8 * Rand(0.9)	84.06	98.41	78.8	97.78

Table 10: Accuracy for the various training paradigms for resnet18 trained on imagewoof

Training with resnet50 on imagewoof					
Training paradigm	Masking matrix (M)	top-1 full	top-5 full	top-1 small	top-5 small
Standard-full		85.2	98.4		
Standard-full + dropout (0.75)		82.76	98.38		
Adjoint-4	Adj-4	85.52	98.3	85.26	98.17
Adjoint-8	Adj-8	85.62	98.59	84.11	98.35
Adjoint-16	Adj-16	85.28	98.54	82.94	98.12
Adjoint-4	Adj-4 * Rand(0.5)	85.75	98.48	85	98.48
Adjoint-4	Adj-4 * Rand(0.6)	85.75	98.69	85.15	98.54
Adjoint-4	Adj-4 * Rand(0.7)	85.31	98.38	84.5	98.35
Adjoint-4	Adj-4 * Rand(0.8)	85.65	98.64	84.76	98.43
Adjoint-4	Adj-4 * Rand(0.9)	86.3	98.59	84.27	98.48
Adjoint-8	Adj-8 * Rand(0.5)	85.72	98.67	83.95	98.28
Adjoint-8	Adj-8 * Rand(0.6)	85.62	98.64	84.01	98.41
Adjoint-8	Adj-8 * Rand(0.7)	85.62	98.48	83.3	98.35
Adjoint-8	Adj-8 * Rand(0.8)	85.49	98.51	82.52	98.38
Adjoint-8	Adj-8 * Rand(0.9)	85.65	98.75	83.41	98.33
Adjoint-16	Adj-16 * Rand(0.5)	86.01	98.56	83.09	98.25
Adjoint-16	Adj-16 * Rand(0.8)	85.39	98.61	82.73	98.12
Adjoint-16	Adj-16 * Rand(0.9)	85.33	98.67	82.26	98.38

Table 11: Accuracy for the various training paradigms for resnet50 trained on imagewoof

C.5 Experiments on oxford-pets

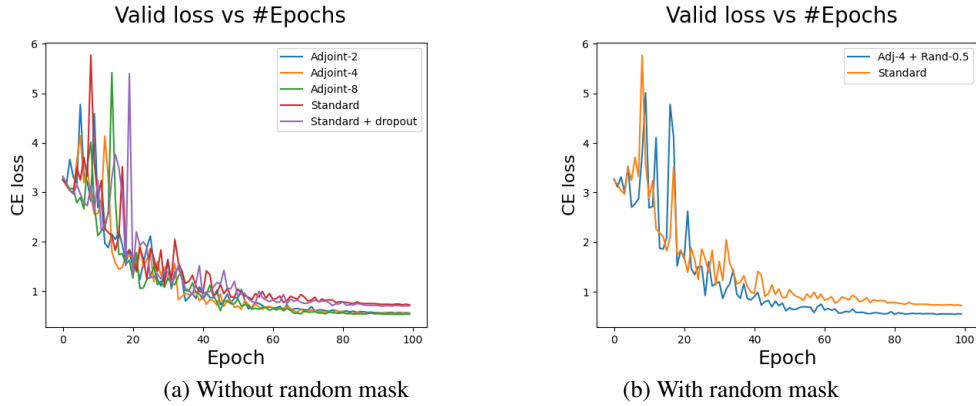


Figure 21: Validation loss for the various training paradigms for resnet50 trained on oxford-pets All the adjoint plots correspond to the bigger network.

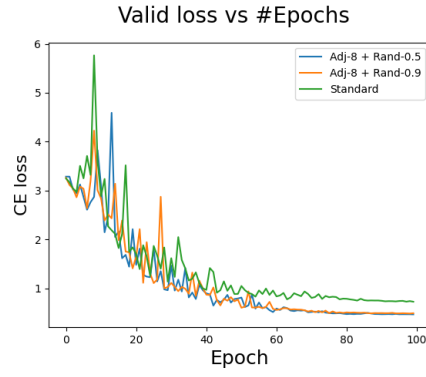
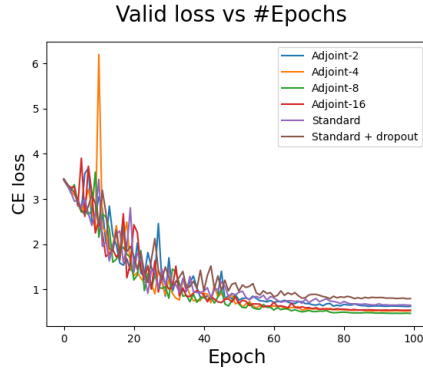
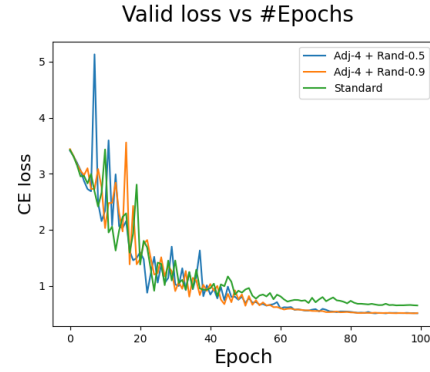


Figure 22: Validation loss for the various training paradigms for resnet50 trained on oxford-pets. All the adjoint plots correspond to the bigger network.

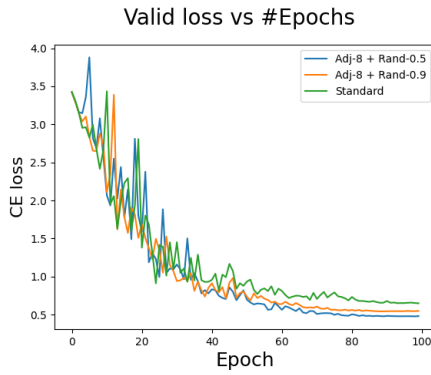


(a) Without random mask

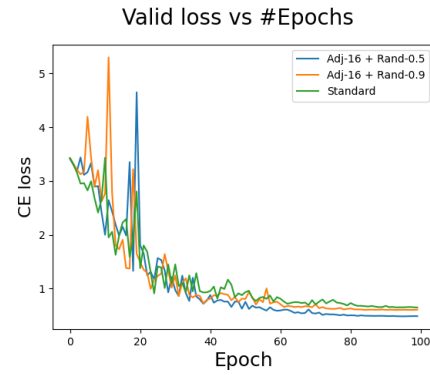


(b) With random mask

Figure 23: Validation loss for the various training paradigms for resnet18 trained on oxford-pets. All the adjoint plots correspond to the bigger network.



(a)



(b)

Figure 24: Validation loss for the various training paradigms for resnet18 trained on oxford-pets. All the adjoint plots correspond to the bigger network.

Training with resnet50 on oxford-pets					
Training paradigm	Masking matrix (M)	top-1 full	top-5 full	top-1 small	top-5 small
Standard-full		85.31	97.63		
Standard-full + dropout (0.5)		84.7	98.1		
Adjoint-2	Adj-2	87	98.03	86	98.1
Adjoint-4	Adj-4	86.73	98.24	85.58	98.03
Adjoint-8	Adj-8	85.85	98.24	84.03	98.1
Adjoint-2	Adj-2 * Rand(0.5)	86.6	97.22	85.85	97.36
Adjoint-2	Adj-2 * Rand(0.9)	85.52	98.17	85.58	97.69
Adjoint-4	Adj-4 * Rand(0.5)	86.12	97.9	85.38	97.56
Adjoint-4	Adj-4 * Rand(0.9)	85.25	97.63	83.69	97.69
Adjoint-8	Adj-8 * Rand(0.5)	86.33	98.37	84.64	97.63
Adjoint-8	Adj-8 * Rand(0.9)	85.85	98.37	81.93	98.51

Table 12: Accuracy for the various training paradigms for resnet50 trained on oxford-pets

Training with resnet18 on oxford-pets					
Training paradigm	Masking matrix (M)	top-1 full	top-5 full	top-1 small	top-5 small
Standard-full		84.84	97.76		
Standard-full + dropout (0.5)		82.61	97.09		
Adjoint-2	Adj-2	84.5	97.56	83.89	97.36
Adjoint-4	Adj-4	86.33	98.3	83.08	97.76
Adjoint-8	Adj-8	85.52	98.71	82.61	97.97
Adjoint-2	Adj-2 * Rand(0.5)	84.91	97.69	83.62	97.63
Adjoint-2	Adj-2 * Rand(0.9)	83.76	97.76	80.71	97.22
Adjoint-4	Adj-4 * Rand(0.5)	85.65	97.9	82.74	97.83
Adjoint-4	Adj-4 * Rand(0.9)	84.84	97.83	80.51	97.09
Adjoint-8	Adj-8 * Rand(0.5)	85.31	97.9	82.07	97.63
Adjoint-8	Adj-8 * Rand(0.9)	83.33	97.9	76.72	96.48
Adjoint-16	Adj-16 * Rand(0.5)	84.5	97.83	77.46	96.75
Adjoint-16	Adj-16 * Rand(0.9)	82.27	97.76	72.05	95.26

Table 13: Accuracy for the various training paradigms for resnet18 trained on oxford-pets